

Meson and Baryon dispersion relations with Brillouin fermions

Stephan Dürr ^{a,b}, Giannis Koutsou ^c and Thomas Lippert ^{a,b}

^a*Bergische Universität Wuppertal, Gaußstraße 20, 42119 Wuppertal, Germany*

^b*Jülich Supercomputing Center, Forschungszentrum Jülich, 52425 Jülich, Germany*

^c*Cyprus Institute, CaSToRC, 20 Kavafi Street, Nicosia 2121, Cyprus*

Abstract

We study the dispersion relations of mesons and baryons built from Brillouin quarks on one $N_f = 2$ gauge ensemble provided by QCDSF. For quark masses up to the physical strange quark mass, there is hardly any improvement over the Wilson discretization, if either action is link-smeared and tree-level clover improved. For quark masses in the range of the physical charm quark mass, the Brillouin action still shows a perfect relativistic behavior, while the Wilson action induces severe cut-off effects. As an application we determine the masses of the Ω_c^0 , Ω_{cc}^+ and Ω_{ccc}^{++} baryons on that ensemble.

1 Introduction

Wilson fermions offer an effective way of regulating the quark sector of QCD. Their conceptual simplicity entails a one-to-one correspondence between lattice and continuum flavor, a property which is particularly convenient for studying flavor physics in the Standard model or in one of its extensions. The main disadvantage is that they induce cut-off effects in physical observables which are both parametrically and numerically large, i.e. $\propto a$, where a is the lattice spacing, and the prefactor is sizable (for a discussion see e.g. the recent review [1]).

Two technical remedies which have proven useful in mitigating the discretization effects are clover improvement and link smearing. The first one changes the parametric behavior to anything between $\alpha^n a$ and a^2 (α is the strong coupling constant) [2], depending on whether the coefficient c_{SW} in (1) is adjusted in perturbation theory or non-perturbatively [3]. The second one concerns the links that enter the Dirac operator, in the covariant derivative and/or the clover term, and reduces the coefficient that multiplies the cut-off terms [4–8]. It turns out that either idea greatly enhances the others effectiveness [9]; by combining a generic overall link smearing with an un-sophisticated improvement strategy (e.g. the tree-level choice $c_{\text{SW}} = 1$) the amount of chiral symmetry breaking becomes as small as $am_{\text{res}} = O(10^{-2})$ [9, 10].

In recent years such tree-level improved fat-link Wilson fermions have proved extremely successful, in particular in enabling simulations of QCD with $N_f = 2 + 1$ dynamical fermions directly at the physical mass point [11] (for an overview of the physics results obtained with such studies see [1]). One can ask whether further action improvements would warrant the

potential increase in CPU time needed to solve the Dirac equation $Dx = b$ for a given right-hand side b . The goal of this paper is to investigate this question for the case of the “Brillouin fermion” proposed in [12]. From the definition of the Wilson and Brillouin actions

$$D^{\text{Wil}}(x, y) = \sum_{\mu} \gamma_{\mu} \nabla_{\mu}^{\text{std}}(x, y) - \frac{1}{2} I \Delta^{\text{std}}(x, y) + \frac{1}{2\kappa} \delta_{x,y} - \frac{c_{\text{SW}}}{2} \sum_{\mu < \nu} \sigma_{\mu\nu} F_{\mu\nu} \delta_{x,y} \quad (1)$$

$$D^{\text{Bri}}(x, y) = \sum_{\mu} \gamma_{\mu} \nabla_{\mu}^{\text{iso}}(x, y) - \frac{1}{2} I \Delta^{\text{bri}}(x, y) + \frac{1}{2\kappa} \delta_{x,y} - \frac{c_{\text{SW}}}{2} \sum_{\mu < \nu} \sigma_{\mu\nu} F_{\mu\nu} \delta_{x,y} \quad (2)$$

it is clear that the new fermion discretization is structurally close to the Wilson variety, except that the covariant derivative and the Laplacian are chosen to minimize the amount of rotational symmetry breaking (which led to an operator which is quite close to the one of Ref. [13], in spite of the construction being based on rather different principles).

The remainder of this article is organized as follows. In Sec. 2 we specify the set of $N_f = 2$ gauge field configurations that we use to carry out our investigation, and we give further details of the link smearing and clover improvement (which we use both in the Wilson and in the Brillouin action, to compare like with like). Next, Sec. 3 contains the precise form of the Wuppertal smearing that we apply on both the source and the sink side of our propagators, and describes the procedure by which we tune the mass parameters κ in (1, 2) to the correct value for the light, strange and charm quark mass. Sec. 4 contains the central piece of our investigation, a comparison of the dispersion relation $E(\mathbf{p})^2$ as a function of the spatial momentum \mathbf{p}^2 for mesons and baryons built from Wilson and Brillouin fermions. As a phenomenological application, we compare in Sec. 5 the mass of the Ω_c^0 baryon that we find to experiment, and we give the masses of the hitherto unobserved states Ω_{cc}^+ and Ω_{ccc}^{++} on the ensemble considered. We summarize our findings in Sec. 6, and arrange details of the baryon interpolating fields in an appendix.

2 Ensemble and valence action details

The goal of our investigation is to compare the Wilson (1) and Brillouin (2) fermion actions in the valence sector, with special emphasis on the dispersion relation $E^2 = E^2(\mathbf{p}^2)$ for mesons and baryons composed of such quarks. We shall use a freely available set of dynamical gauge field configurations, i.e. with the effect of light sea quark loops included. We select an ensemble out of the $N_f = 2$ collection by QCDSF [14], namely the one with

$$\beta = 5.29, \quad L/a = 40, \quad T/a = 64, \quad \kappa_{ud}^{\text{sea}} = 0.13632 \quad (3)$$

and $aM_{\pi}^{\text{sea}} = 0.1034(8)$ [14]. Thus $M_{\pi}^{\text{sea}}L = 4.136$, which bears the promise of small finite-size effects. QCDSF determines the scale of their $\beta = 5.29$ ensembles to be $a^{-1} = 2.71(2)(7)$ [15], tantamount to $a = 0.0728(5)(19)$ fm, which implies $M_{\pi}^{\text{sea}} \simeq 280$ MeV and $L \simeq 2.9$ fm.

Either action involves 3-fold APE smeared gauge links, where one smearing step in $d = 4$ space-time dimensions is given by

$$V_{\mu}(x) = P_{SU(3)} \left\{ (1-\alpha) U_{\mu}(x) + \frac{1}{2(d-1)} \sum_{\pm\nu \neq \mu} U_{\nu}(x) U_{\mu}(x+\hat{\nu}) U_{\nu}^{\dagger}(x+\hat{\mu}) \right\} \quad (4)$$

and we use $\alpha_{4D} = 0.72$. Here $P_{SU(3)}$ denotes the back-projection to $SU(3)$ as described in [12] and U is the unsmeared (original) gauge field. Note that these four-dimensionally smeared links

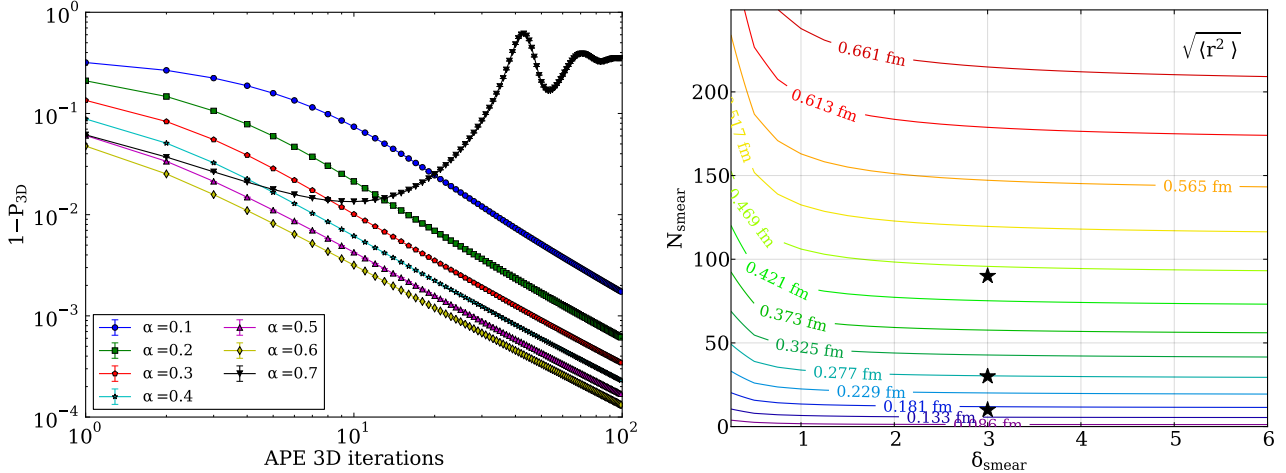


Figure 1: *Left:* $1 - \langle \text{ReTr}(U_{\text{spat}}) \rangle / 3$ versus the number of 3D APE smearings for various values of α_{3D} ; the perturbative bound is $\alpha_{3D} < 2/3$ [9]. *Right:* contour plot of $\langle r^2 \rangle^{1/2}$ of a Wuppertal smeared quark source; the asterisks refer to Fig. 2. Either plot is based on 5 configurations.

enter both the (relevant) covariant derivative and the (irrelevant) clover term of the Wilson and Brillouin operators (for a summary of the options see [9], but this choice is the simplest and, as far as we can see, the most effective one). In addition, the clover coefficient is set to its tree-level value ($c_{\text{sw}} = 1$) for either action. In short, this is the same action as used in [12], except that we now use three steps of APE smearing rather than one.

3 Wuppertal smearing and quark mass tuning

Wuppertal smearing amounts to the spreading of a vector $q(\mathbf{x}, t)$ – with non-trivial support on the time-slice t – within that time-slice by means of N_W operations of the form [16]

$$q(\mathbf{x}, t) \quad \longrightarrow \quad \frac{\delta_{\mathbf{x}, \mathbf{y}} + \delta_W \sum_i \{ V_i(\mathbf{x}, t) \delta_{\mathbf{x} + \hat{i}, \mathbf{y}} + V_i^\dagger(\mathbf{x} - \hat{i}, t) \delta_{\mathbf{x} - \hat{i}, \mathbf{y}} \}}{1 + 6\delta_W} q(\mathbf{y}, t) \quad (5)$$

with spreading parameter δ_W . The index i runs over the three spatial directions, and an implicit summation over \mathbf{y} takes place. Here the spatial links $V_i(\mathbf{x}, t)$ are to be generated with the three-dimensional version of the APE smearing (4) applied to the time-slice t . After the Dirac equation $Dp = q$ has been solved with the broadened source q , an identical spreading is applied to the solution p (for each time-slice separately), i.e. we use smeared-smeared propagators with the same smearing on the source and on the sink side.

In principle Wuppertal smearing has four parameters to adjust, namely (N_{3D}, α_{3D}) of the three-dimensional APE smearing that the spatial links $V_i(\mathbf{x}, t)$ have undergone, and (N_W, δ_W) in the recipe (5). For convenience we try to optimize the two pairs separately.

We first study the behavior of the spatial plaquette of the lattices (3) under repeated applications of the three-dimensional version of the APE recipe (4). Our results are displayed in the left panel of Fig. 1. In [9] there is the perturbative stability bound $\alpha^{\text{APE}} < (d-1)/d$ in d space-time dimensions. Our results suggest that any $\alpha_{3D}^{\text{APE}} < \alpha_{3D}^{\text{crit}}$ induces, asymptotically, a power-law fall-off of $1 - P_{3D}$, and thus allows to drive the 3D-plaquette arbitrarily small.

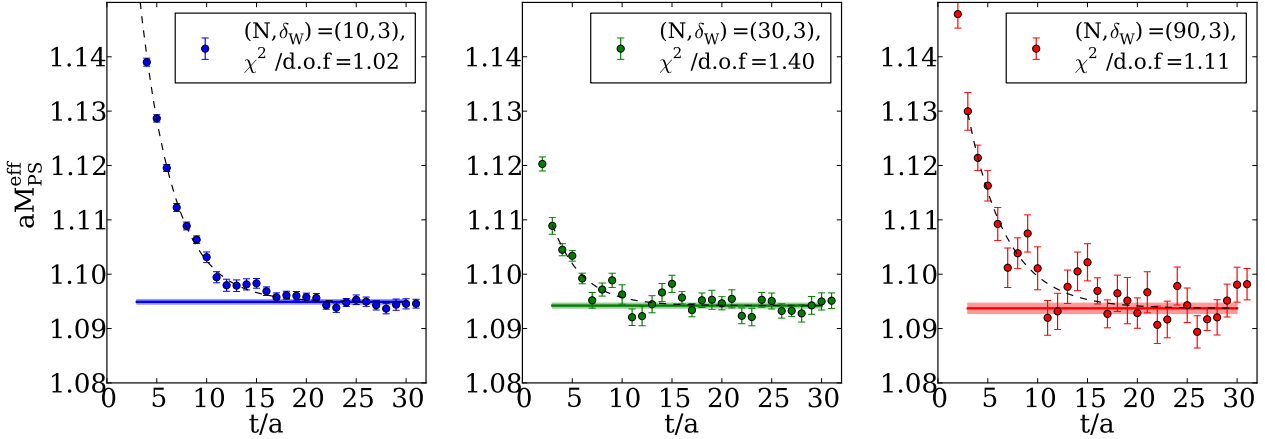


Figure 2: Effective mass of the pseudoscalar $c\bar{c}$ meson made from Brillouin fermions with $\kappa = 0.112429$ for three different widths (cf. Fig. 1) of the Wuppertal smeared sources and sinks.

In addition, $\alpha_{3D}^{\text{crit}}$ seems not too far from the perturbative prediction of $2/3$ [9]. Hence, our recommendation is to apply a large number of 3D APE smearings on the spatial links that enter the Wuppertal spreading (5), e.g. $(N_{3D}, \alpha_{3D}) = (300, 0.6)$ or $(1000, 0.6)$.

To decide on the second pair (N_W, δ_W) in (5) we first consider the root-mean-square (rms) radius of the smeared source as a function of these parameters, the former being defined through

$$\langle r^2 \rangle = \frac{\sum_{\mathbf{r}} \mathbf{r}^2 q^\dagger(\mathbf{r}) q(\mathbf{r})}{\sum_{\mathbf{r}} q^\dagger(\mathbf{r}) q(\mathbf{r})}. \quad (6)$$

Results from 5 configurations are shown in the right panel of Fig. 1. As expected, the contours look like hyperbolas, that is the rms radius of q is in the first place a function of the product $N_W \delta_W$. Next, we consider the effective mass of a meson made from $\kappa = 0.112429$ Brillouin fermions (which is in the vicinity of κ_c^{Bri} , see below) for $(N_W = 10, 30, 90, \delta_W = 3)$, with results presented in Fig. 2. In this range, a higher iteration count appears not to decrease the coupling to excited states, but rather seems to induce more noise in the correlators. As a consequence we decide to stay with the conservative parameter set $(N_W = 10, \delta_W = 0.5)$.

To compare like with like, we wish to compare the dispersion relation for mesons and baryons put together from Wilson and Brillouin fermions at a fixed value of the light, strange or charm quark mass. This is most conveniently done by first tuning the two κ -values to get common values of aM_π , $aM_{s\bar{s}}$ and $aM_{c\bar{c}}$, respectively, for either discretization. For the mesons we use the PP correlators, and given their cosh-form it is advantageous to define the effective mass as

$$aM_{\text{eff}}(t) = \frac{1}{2} \log \left(\frac{C(t-1) + \sqrt{C(t-1)^2 - C(T/2)^2}}{C(t+1) + \sqrt{C(t+1)^2 - C(T/2)^2}} \right) \quad (7)$$

because this modification remedies the fall-off that the effective mass would show near the center of the box if the generic definition

$$aM_{\text{eff}}(t) = \frac{1}{2} \log \left(\frac{C(t-1)}{C(t+1)} \right) \quad (8)$$

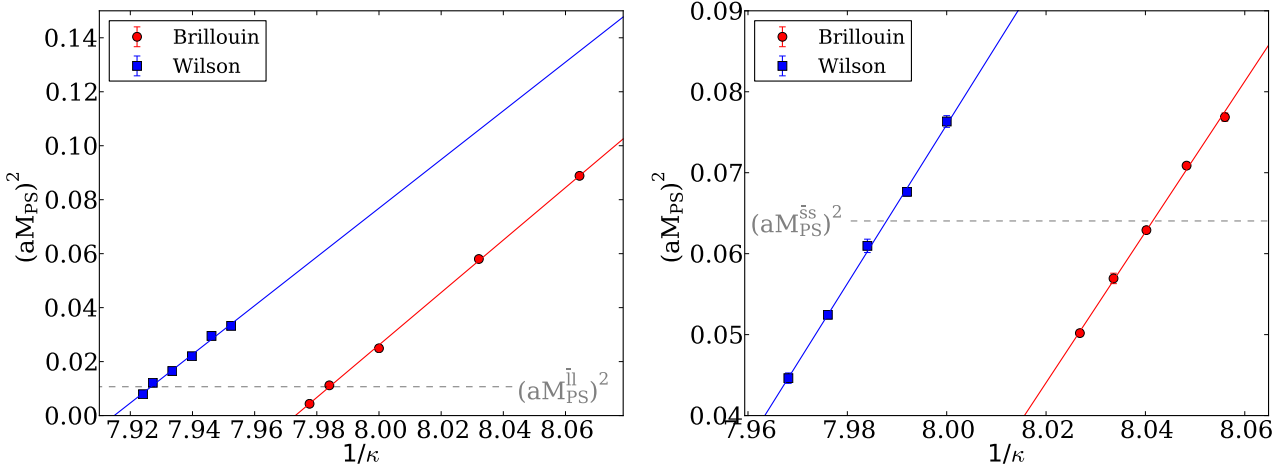


Figure 3: *Left:* Tuning of κ_l to achieve $(aM_P)^2 = 0.01069$ with either action. *Right:* Similar tuning of κ_s to achieve $(aM_P)^2 = 0.06404$.

would be used. For baryons with (exact or approximate) projection to a definite parity (see Sec. 4 below) we use the latter form, since these correlators do not show the cosh form.

For the light quark we demand the pion mass to be the same (in lattice units) as in the sea, that is $(aM_P)^2 = 0.01069$, given the information provided beneath (3). We solve the Dirac equation for a few κ -values in the vicinity of the suspected target value, and interpolate them linearly to obtain the desired κ_l , as shown in the left panel of Fig. 3. The results read

$$\kappa_l^{\text{Bri}} = 0.125249, \quad \kappa_l^{\text{Wil}} = 0.126146. \quad (9)$$

For the strange quark we use the scale provided below (3) and the value $M_{s\bar{s}} = 0.6858(7)$ GeV which follows via $\sqrt{2M_K^2 - M_\pi^2}$ from the isospin-averaged and electromagnetically corrected masses $M_\pi = 134.8(3)$ MeV and $M_K = 494.2(5)$ MeV [17]. This gives the target value $(aM_P)^2 = 0.06404$, and a similar interpolation procedure, shown in the right panel of Fig. 3, yields

$$\kappa_s^{\text{Bri}} = 0.1251902, \quad \kappa_s^{\text{Wil}} = 0.1243560. \quad (10)$$

For the charm quark we proceed analogously to the strange case, except that we now use the value $M_{c\bar{c}} = 2.9810(11)$ GeV from PDG [18]. This yields the target value $(aM_P)^2 = 1.210$, and with essentially the same kind of procedure we find

$$\kappa_c^{\text{Bri}} = 0.112336, \quad \kappa_c^{\text{Wil}} = 0.112513. \quad (11)$$

A careful look at the left panel of Fig. 3 reveals that one of our trial κ_l -values for the Brillouin action happens to be rather light; for this point we find $aM_\pi = 0.067(5)$, tantamount to $M_\pi \simeq 180$ MeV. Following [11, 19] we monitor the inverse iteration count of the solver (which is a proxy for the smallest eigenvalue of $D^\dagger D$) to make sure that we do not run into an “exceptional configuration” problem. The results of this monitoring are displayed in Fig. 4. Even for the lightest quark mass the distribution is roughly Gaussian, and the origin is 3 to 4 standard deviations away from the median. This shows that even in this strongly non-unitary regime (where M_π^{val} is about 100 MeV lighter than M_π^{sea}) the Brillouin operator can be safely inverted. We consider this an encouraging sign of the great stability of our action against fluctuations of the small eigenmodes, and think that this stability has the potential to render the Brillouin operator a cheap alternative to overlap or domain-wall fermions.

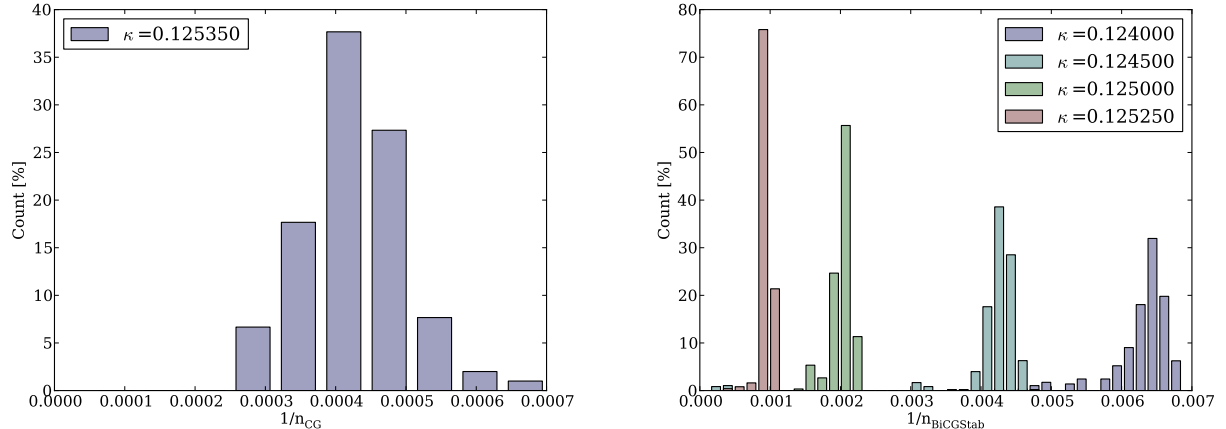


Figure 4: Iteration count of the inversions with the trial κ_l of Fig. 3 for the Brillouin action, using the CG (left) and the BiCGstab (right) algorithm for the lightest and all but the lightest masses, respectively. In each case $O(25)$ configurations are used.

4 Meson and baryon dispersion relations

With the tuned $\kappa_l, \kappa_s, \kappa_c$ of (9, 10, 11) in hand, we are now in a position to study the dispersion relation $E^2 = E^2(\mathbf{p}^2)$ for mesons and baryons composed of either Brillouin or Wilson fermions.

To this end we consider two-point correlators of the form

$$C_M(t, \mathbf{p}) = \sum_{\mathbf{x}} \langle J_M(\mathbf{x}, t) \bar{J}_M(\mathbf{0}, 0) \rangle e^{i\mathbf{p}\mathbf{x}} \quad (12)$$

$$C_B^\pm(t, \mathbf{p}) = \text{Tr } \frac{1}{2}(1 \pm \gamma_4) \sum_{\mathbf{x}} \langle J_B(\mathbf{x}, t) \bar{J}_B(\mathbf{0}, 0) \rangle e^{i\mathbf{p}\mathbf{x}} \quad (13)$$

where M and B define the quantum numbers of the meson or baryon, respectively. For non-zero momentum the correct parity projector in (13) would read $\frac{1}{2}(1 \pm \frac{E}{M}\gamma_4)$ [20, 21], but we stay with the simpler form, since we are always interested in the lower-mass parity partner (which requires no projection at all). Finally, the sink and the source in (13) contain an uncontracted spinor index, say μ and ν . The projection to a definite spin can be done with [22]

$$(P^{3/2})_{\mu\nu} = \delta_{\mu\nu} - \frac{1}{3}\gamma_\mu\gamma_\nu - \frac{1}{3p^2}(\not{p}\gamma_\mu p_\nu - p_\mu\gamma_\nu\not{p}) \quad (14)$$

$$(P_{11}^{1/2})_{\mu\nu} = \frac{1}{3}\gamma_\mu\gamma_\nu - \frac{1}{p^2}p_\mu p_\nu + \frac{1}{3p^2}(\not{p}\gamma_\mu p_\nu - p_\mu\gamma_\nu\not{p}) \quad (15)$$

and similar expressions for $P_{12,21,22}^{1/2}$ as given in eqn. (9) of [22]. For $\mathbf{p} = 0$ they simplify to

$$(P^{3/2})_{ij} = \delta_{ij} - \frac{1}{3}\gamma_i\gamma_j \quad (16)$$

$$(P_{11}^{1/2})_{ij} = \frac{1}{3}\gamma_i\gamma_j \quad (17)$$

which are easy to implement and good enough for many purposes (we are always interested in the lowest-mass state). For details of (more advanced) spin projection see [23].

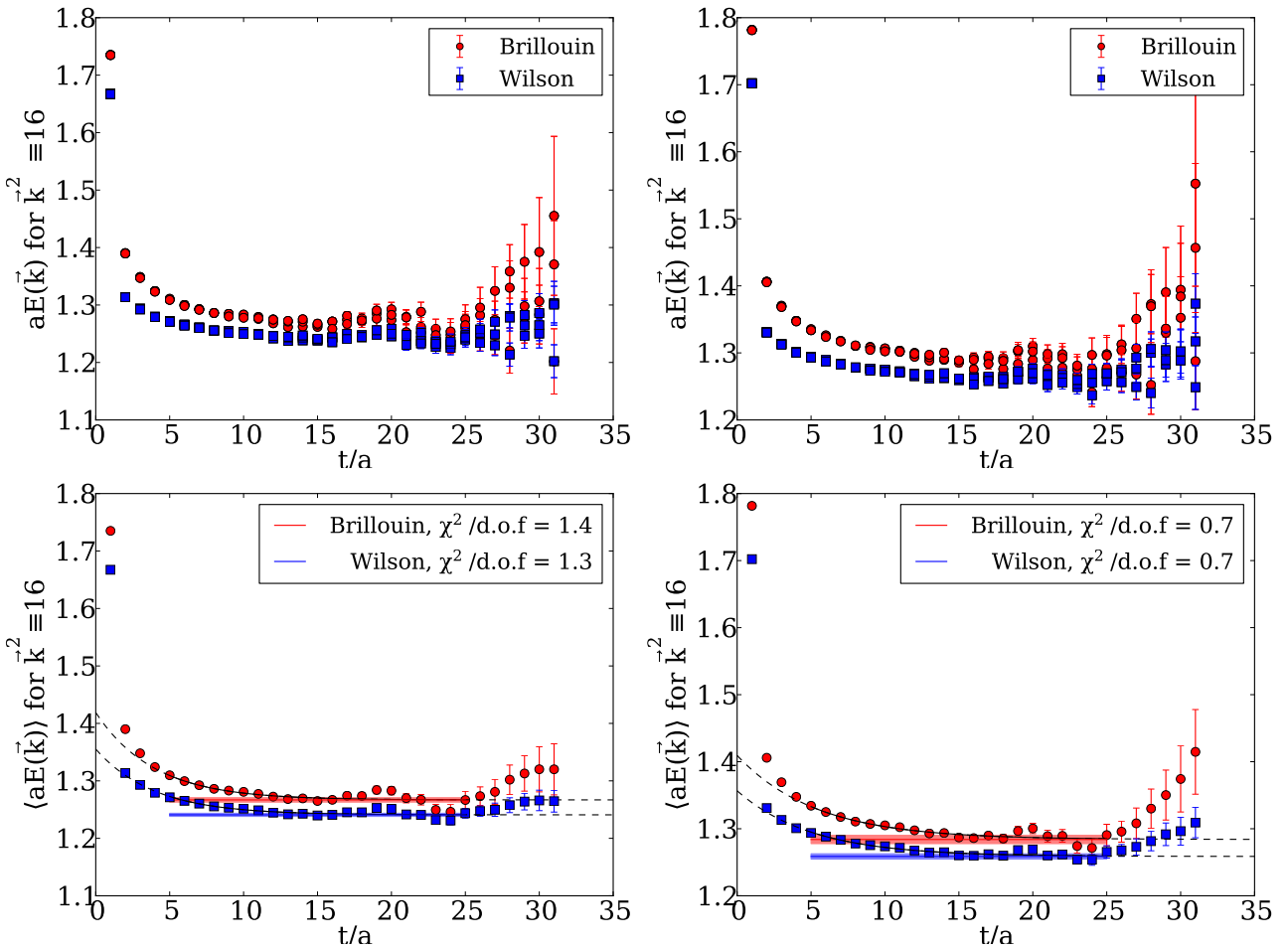


Figure 5: Effective mass plots of the pseudoscalar (left) and vector (right) $c\bar{c}$ meson before (top) and after (bottom) averaging over the \mathbf{k} -configurations that contribute to $\mathbf{k}^2 = 16$.

Having defined the correlation functions, we can now move on to the dispersion relations. We consider spatial momenta $\mathbf{p} = 2\pi/L \cdot \mathbf{k}$ with $0 \leq \mathbf{k}^2 \leq 20$. Thanks to the cubic symmetry among the spatial directions, in general several \mathbf{k} -configurations contribute to a given \mathbf{k}^2 . An effective mass plot before and after taking an average over the various contributions is shown in Fig. 5, for the pseudoscalar and vector meson, in the case of $\mathbf{k}^2 = 16$. We see no big discrepancies before the average is taken, hence the averaging seems justified.

Repeating this procedure for all \mathbf{k}^2 yields the data presented in Fig. 6. We show the dispersion relations for the pseudoscalar and the vector meson with quark content $s\bar{s}$ (top), $s\bar{c}$ (middle), $c\bar{c}$ (bottom). Evidently, for the heavier masses there is a significant difference between the Wilson data (red circles) and those with the Brillouin discretization (blue squares). The full black line is not a fit, but the relativistic dispersion relation $E^2 = \mathbf{p}^2 + M^2$, starting from the first data-point (where the two actions were tuned to yield the same result for the $s\bar{s}$ and $c\bar{c}$ pseudoscalar states, but not for the remaining four states). This line shows that the discretization effects are induced by the Wilson action; within statistical errors the Brillouin data are free from such effects.

Similarly, we can work out the dispersion relations for baryons. The data for the “decuplet-type” states $\Omega_{sss}^-, \Omega_{ccc}^{++}$ [which form a 20-plet under $SU(4)$], as well as for the “octet-type”

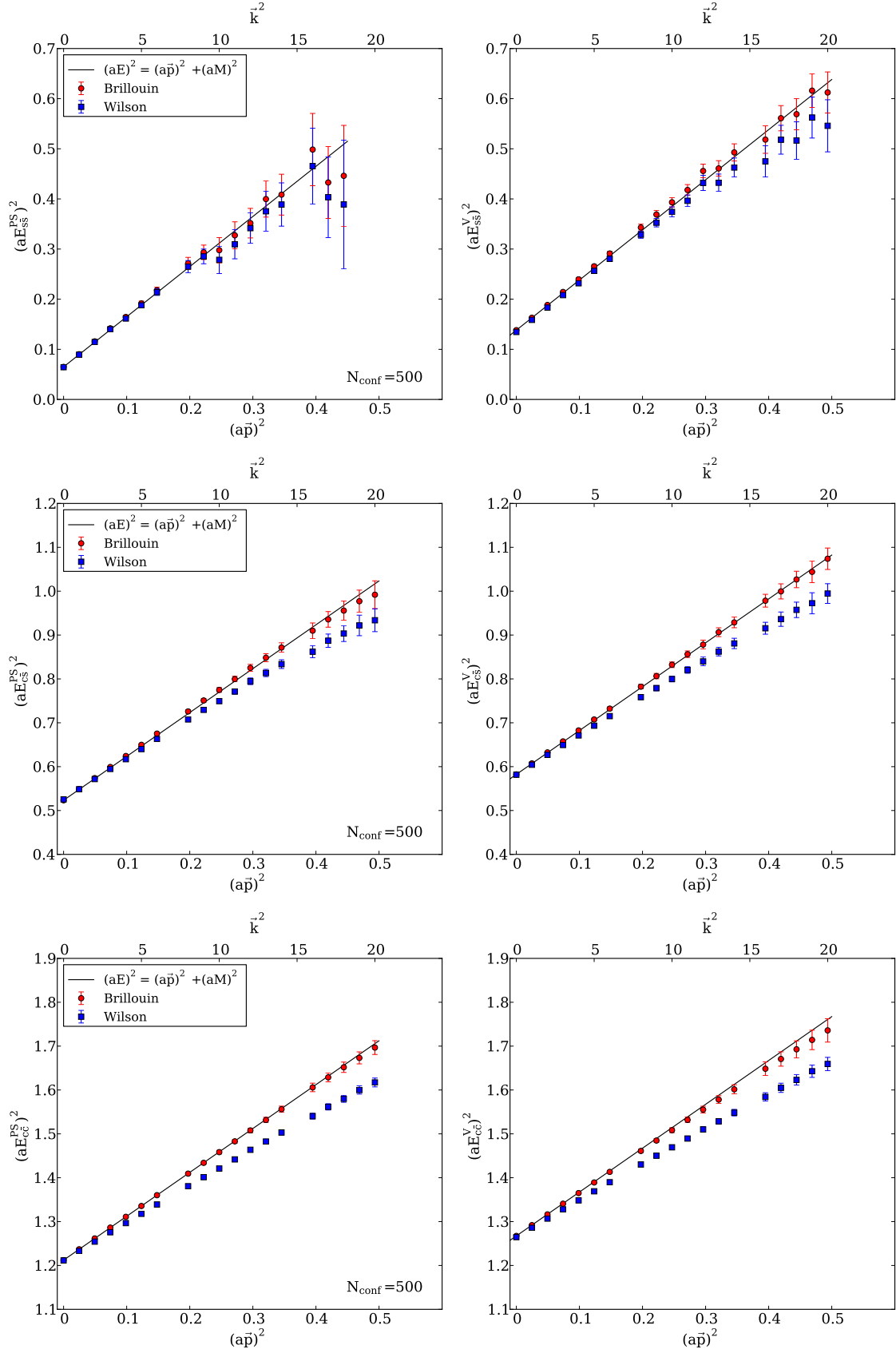


Figure 6: Dispersion relations for the pseudoscalar (left) and vector (right) meson with $s\bar{s}$ (top), $s\bar{c}$ (middle), $c\bar{c}$ (bottom) quark content. The black line shows the relativistic $E^2 = \mathbf{p}^2 + M^2$.

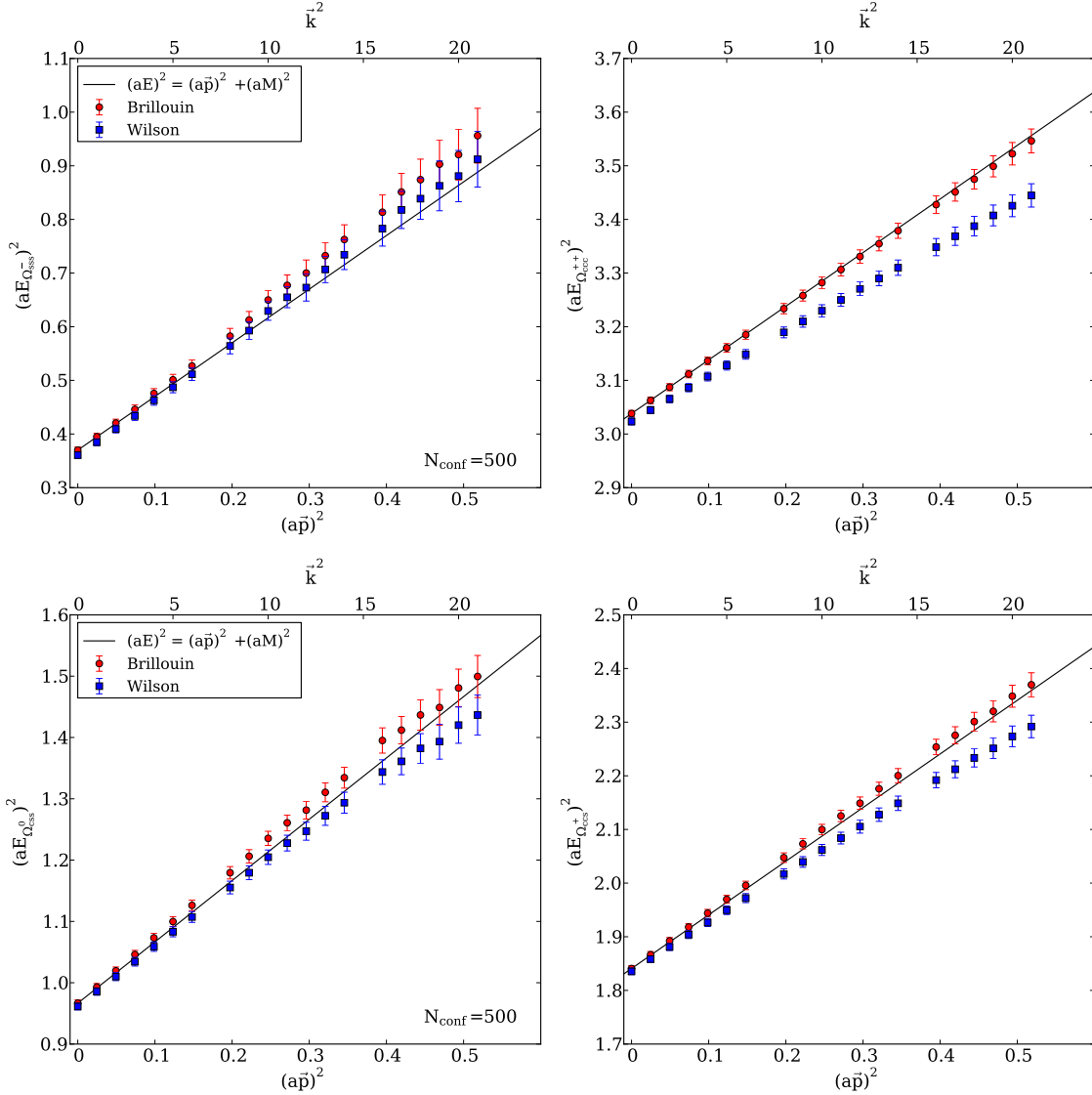


Figure 7: Dispersion relations for the decuplet-type Ω_{sss}^- , Ω_{ccc}^{++} (top left and right) and the octet-type Ω_{css}^0 , Ω_{ccs}^+ (bottom left and right). The black line shows the relativistic $E^2 = \mathbf{p}^2 + M^2$.

states Ω_{css}^0 , Ω_{ccs}^+ [which form a 20'-plet under SU(4)] are shown in Fig. 7. To make it clear which states we consider, the interpolating fields of both the 20-plet and the 20'-plet are listed in the appendix. Again, the full black line is not a fit but the relativistic dispersion relation $E^2 = \mathbf{p}^2 + M^2$, and we stress that no further tuning of κ -values was performed. Just like in the meson case, we see no significant difference in the regime of the physical strange quark mass (which explains why we refrain from looking at even lighter κ values, such data would just be more noisy). However, with every strange quark that is replaced by a charm quark, the difference becomes more pronounced, up to the point where the dispersion relation of the Ω_{ccc}^{++} is seriously distorted with Wilson fermions, but relativistically correct with Brillouin fermions.

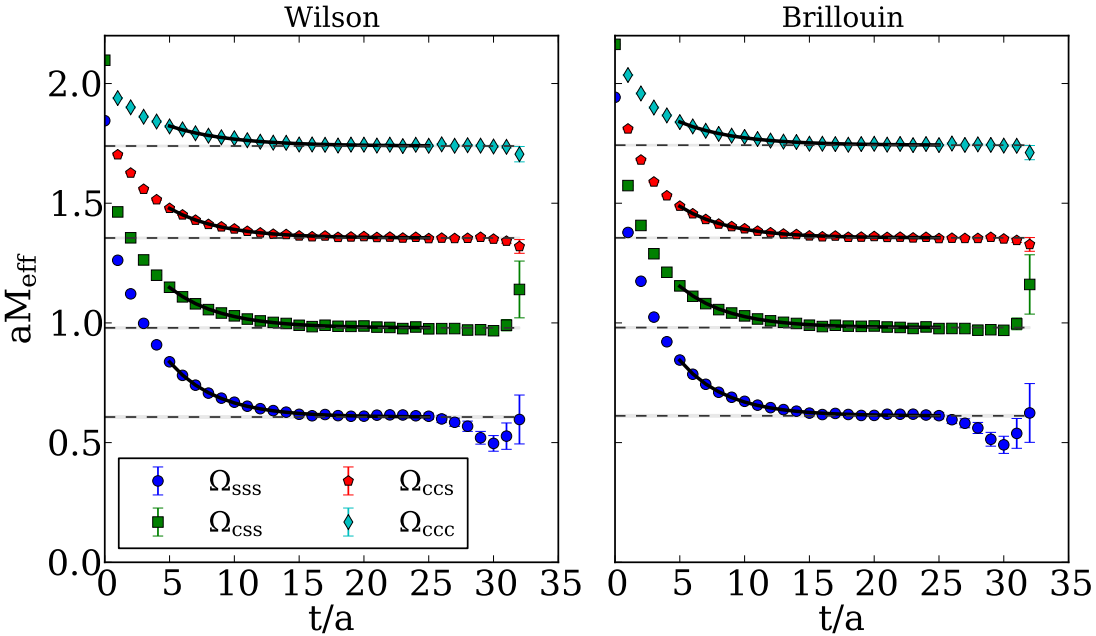


Figure 8: Effective masses of the Ω_{sss} , Ω_{ccc} (decuplet-type states) and Ω_{ssc} , Ω_{ccc} (octet-type states) at $\mathbf{p} = 0$ for the Wilson (left) and Brillouin (right) action.

combination	Wilson	Brillouin
$(\Omega_{css} - \Omega_{sss})/\Omega_{sss}$	0.616(8)	0.604(8)
$(\Omega_{ccs} - \Omega_{css})/\Omega_{sss}$	0.617(6)	0.612(6)
$(\Omega_{ccc} - \Omega_{ccs})/\Omega_{sss}$	0.633(5)	0.633(5)
$(\Omega_{ccs} - \Omega_{css})/\Omega_{css}$	0.383(3)	0.382(3)
$(\Omega_{ccc} - \Omega_{ccs})/\Omega_{ccs}$	0.284(1)	0.286(1)

Table 1: Relative mass splittings between the various Ω states, as determined with the Wilson (left) and the Brillouin (right) action. Here, the symbol Ω_{xyz} is meant as a shorthand for $M_{\Omega_{xyz}}$.

5 Masses of multiply charmed baryons

As a byproduct of our investigation, and with the goal of spurring further improvements, we can quote the masses of the Ω baryons considered in the previous section. Let us emphasize that this activity is based on the single ensemble (3). We will try to minimize the systematic effects on the numbers given below, but there is no way of reliably assessing the size of such systematic effects, given the data that we have.

Let us begin by showing the effective mass plots of the four states Ω_{sss}^- , Ω_{css}^0 , Ω_{ccs}^+ , Ω_{ccc}^{++} in Fig. 8. This is at $\mathbf{p} = 0$, and we see no significant difference between the Wilson and the Brillouin action. Let us recall that the tuning was done in the meson sector, so this is a first non-trivial observation. To minimize the systematics it is usually a good idea to look at mass splittings, and to form dimensionless ratios. The former trick mitigates the effect of excited states contaminations and possible finite volume effects, the latter one reduces the sensitivity to the overall scale. The effective mass plots for all adjacent mass splittings, based on ratios of correlators like $\langle C_{css} \rangle / \langle C_{sss} \rangle$, are shown in Fig. 9. Even at this level of zoom, the quality of the

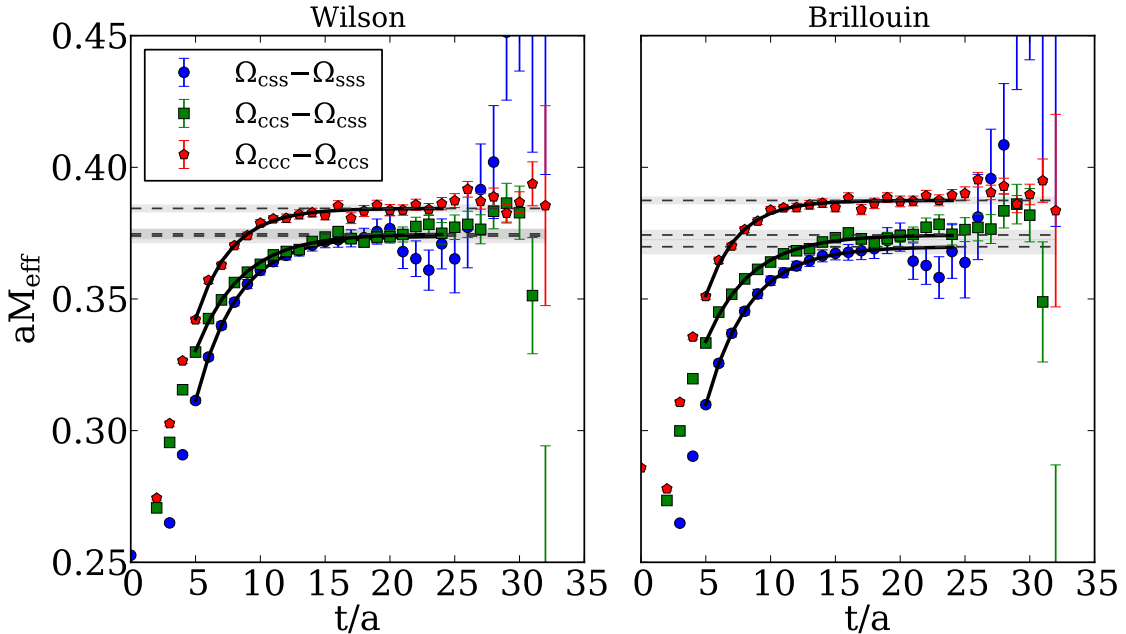


Figure 9: Same as Fig. 8, but for the splittings $M_{\Omega_{css}} - M_{\Omega_{sss}}$ and $M_{\Omega_{ccs}} - M_{\Omega_{css}}$ and $M_{\Omega_{ccc}} - M_{\Omega_{ccs}}$.

data appears rather good, and we see only very mild differences between the Wilson and the Brillouin data. We list the relative mass splittings (normalized both with the lower one of the two states involved and with the $\Omega^- = \Omega_{sss}$ base state) in Tab. 1.

Regarding phenomenological numbers, we should first mention that the experimental mass of the Ω^- (i.e. the $J^P = 3/2^+$, $c = 0$, $s = 3$ state in Tab. 3) is 1672.45(29) MeV, and the mass of the Ω_c^0 (i.e. the $J^P = 1/2^+$, $c = 1$, $s = 2$ state in Tab. 2) is 2697.5(2.6) MeV [18]. Hence, with the ratios listed in Tab. 1, we can only compare the mass of the Ω_c^0 baryon to experiment, but not the masses of the Ω_{cc}^+ (i.e. the $J^P = 1/2^+$, $c = 2$, $s = 1$ state in Tab. 2) and of the Ω_{ccc}^{++} (i.e. the $J^P = 3/2^+$, $c = 3$, $s = 0$ state in Tab. 3). We shall use the first three lines in Tab. 1, taking the Brillouin number as our central value and the average difference to the Wilson number (0.006) as a uniform estimate of the systematic error. Adding all errors in quadrature yields

$$M_{\Omega_c^0} = 2.68(2) \text{ GeV} \quad (18)$$

$$M_{\Omega_{cc}^+} = 3.71(2) \text{ GeV} \quad (19)$$

$$M_{\Omega_{ccc}^{++}} = 4.77(3) \text{ GeV} \quad (20)$$

and we emphasize that these errors do not include the effect of the (missing) limits $a \rightarrow 0$ and $M_\pi^{\text{sea}} \rightarrow 134.8$ MeV. Nevertheless, (18) is consistent with experiment, albeit with a large error. From these numbers it appears that the actual splitting is very close to equidistant, a notion which is also conveyed by Fig. 9.

We refrain from comparing our numbers to similar results in the recent literature on charm physics on the lattice [22, 24–34]. We rather like to add that what is really called for, in our opinion, is a complete study with a reasonable assessment of all systematics involved, that is with the continuum limit taken, with an interpolation or extrapolation to the physical values of M_π and M_K in the sea, and with an extrapolation to infinite box volume.

6 Summary

The goal of this work was to test whether a significant difference in meson and baryon dispersion relations is seen, depending on whether such a composite state is built from Wilson or Brillouin fermions. The main result is that for standard lattice spacings ($a^{-1} = 2 - 3 \text{ GeV}$) this is not the case if all quarks are at most as heavy as the physical strange quark, but significant differences become visible if one or several quarks are in the range of the physical charm quark mass – see Fig. 6 for mesons and Fig. 7 for baryons.

The Brillouin operator as proposed in [12] can be seen as a low-cost approximation to the concept of “perfect fermions” [35–38]. A recent development in the field of staggered fermions is to add a mixture of taste-S,V,T,A,P mass terms [39–43] such that the resulting action would have only one or two species in the continuum, and an eigenvalue spectrum similar to the near-Ginsparg-Wilson spectrum of the Brillouin action (see e.g. Fig. 22 of Ref. [12]).

In summary, we reach the conclusion that the added expense, in terms of CPU time, that the Brillouin action entails is hardly justified if one is only interested in light quark spectroscopy (this may be different for structure functions). On the other hand, as soon as charm quarks are involved, the Brillouin action leads to a massive reduction of cut-off effects already in purely spectroscopic quantities. In particular our Fig. 7 shows that the standard lore that aM should not exceed 1 need not be true with Brillouin fermions; in this figure we see no cut-off effects in the range $(aE)^2 = 3.0 - 3.5$. All together, it seems our choice to use the Brillouin action to determine the quark mass ratio m_c/m_s in Ref. [44] was justified, and we hope that this augers well for the accuracy of our results (19, 20).

Acknowledgments: We thank Constantia Alexandrou and Zoltan Fodor for useful discussion. This work was supported in part by DFG through SFB TRR-55. The computing resources for this project were provided by Forschungszentrum Jülich GmbH through a VSR grant.

charm	strange	baryon	interpolating field	I	I_z
$c = 0$	$s = 0$	p	$\epsilon(u^T C \gamma_5 d) u$	1/2	+1/2
		n	$\epsilon(d^T C \gamma_5 u) d$	1/2	-1/2
$s = 1$	Σ^+		$\epsilon(u^T C \gamma_5 s) u$	1	+1
	Σ^0		$\frac{1}{\sqrt{2}} \epsilon \{ (u^T C \gamma_5 s) d + (d^T C \gamma_5 s) u \}$	1	0
	Σ^-		$\epsilon(d^T C \gamma_5 s) d$	1	-1
$s = 2$	Ξ^0		$\epsilon(s^T C \gamma_5 u) s$	1/2	+1/2
	Ξ^-		$\epsilon(s^T C \gamma_5 d) s$	1/2	-1/2
$s = 1$	Λ^0	$\frac{1}{\sqrt{6}} \epsilon \{ 2(u^T C \gamma_5 d) s + (u^T C \gamma_5 s) d - (d^T C \gamma_5 s) u \}$	0	0	
$c = 1$	$s = 0$	Σ_c^{++}	$\epsilon(u^T C \gamma_5 c) u$	1	+1
		Σ_c^+	$\frac{1}{\sqrt{2}} \epsilon \{ (u^T C \gamma_5 c) d + (d^T C \gamma_5 c) u \}$	1	0
		Σ_c^0	$\epsilon(d^T C \gamma_5 c) d$	1	-1
$s = 1$	$\Xi_c'^+$		$\frac{1}{\sqrt{2}} \epsilon \{ (s^T C \gamma_5 c) u + (u^T C \gamma_5 c) s \}$	1/2	+1/2
	$\Xi_c'^0$		$\frac{1}{\sqrt{2}} \epsilon \{ (s^T C \gamma_5 c) d + (d^T C \gamma_5 c) s \}$	1/2	-1/2
$s = 2$	Ω_c^0		$\epsilon(s^T C \gamma_5 c) s$	0	0
$s = 0$	Λ_c^+	$\frac{1}{\sqrt{6}} \epsilon \{ 2(u^T C \gamma_5 d) c + (u^T C \gamma_5 c) d - (d^T C \gamma_5 c) u \}$	0	0	
$s = 1$	Ξ_c^+	$\frac{1}{\sqrt{6}} \epsilon \{ 2(s^T C \gamma_5 u) c + (s^T C \gamma_5 c) u - (u^T C \gamma_5 c) s \}$	1/2	+1/2	
	Ξ_c^0	$\frac{1}{\sqrt{6}} \epsilon \{ 2(s^T C \gamma_5 d) c + (s^T C \gamma_5 c) d - (d^T C \gamma_5 c) s \}$	1/2	-1/2	
$c = 2$	$s = 0$	Ξ_{cc}^{++}	$\epsilon(c^T C \gamma_5 u) c$	1/2	+1/2
		Ξ_{cc}^+	$\epsilon(c^T C \gamma_5 d) c$	1/2	-1/2
$s = 1$	Ω_{cc}^+		$\epsilon(c^T C \gamma_5 s) c$	0	0

Table 2: *Interpolating fields of $SU(4)$ 20'-plet (“octet-type”) baryons with spin 1/2. Throughout the color indices are suppressed, i.e. $\epsilon(x^T C \gamma_5 y) z$ is to be read as $\epsilon_{abc} (x_a^T C \gamma_5 y_b) z_c$.*

Appendix: Charmed baryon interpolating fields

To avoid any confusion to which states our numbers (18-20) would refer to, we give a list of the simplest baryon interpolators with charm and/or strangeness. We follow the naming convention of PDG [18] and group the operators according to their transformation properties under $SU(4)$ in flavor space. Throughout, C denotes the charge conjugation matrix, the transposition sign refers to spinor, and color indices are implicit, as described in the table captions.

Overall, the states separate into a 20'-plet of spin 1/2 states, a 20-plet of spin 3/2 states, and a $\bar{4}$ -plet under $SU(4)$. These states are listed in Tab. 2, Tab. 3, and Tab. 4, respectively.

The 20'-plet decomposes into the standard $c = 0$ ground floor which transforms as an 8 under $SU(3)$ [lines 1-8 in Tab. 2], the $c = 1$ first floor which decomposes into a 6 [lines 9-14] and a $\bar{3}$ [lines 15-17], and the $c = 2$ second floor which transforms as a 3 under $SU(3)$ [lines 18-20]. Regarding the $c = 1$ level, it is worth noticing that the states of the 6 are symmetric under interchange of the two non-charmed quarks, whereas the states of the $\bar{3}$ are antisymmetric under this interchange. Here we adopt the rule that in the 20'-plet the diquark $(x^T C \gamma_5 y)$ is antisymmetric under the interchange $x \leftrightarrow y$.

The structure of the 20-plet is somewhat simpler, since each fixed- c floor has a unique transformation pattern under $SU(3)$. It contains the standard $c = 0$ ground floor which transforms as a 10 under $SU(3)$ [lines 1-10 in Tab. 3], the $c = 1$ first floor which transforms as a 6 [lines 11-16],

charm	strange	baryon	interpolating field	I	I_z
$c = 0$	$s = 0$	Δ^{++}	$\epsilon(u^T C \gamma_\mu u) u$	3/2	+3/2
		Δ^+	$\frac{1}{\sqrt{3}} \epsilon \{ 2(u^T C \gamma_\mu d) u + (u^T C \gamma_\mu u) d \}$	3/2	+1/2
		Δ^0	$\frac{1}{\sqrt{3}} \epsilon \{ 2(d^T C \gamma_\mu u) d + (d^T C \gamma_\mu d) u \}$	3/2	-1/2
		Δ^-	$\epsilon(d^T C \gamma_\mu d) d$	3/2	-3/2
$s = 1$		Σ^{*+}	$\frac{1}{\sqrt{3}} \epsilon \{ 2(u^T C \gamma_\mu s) u + u^T C \gamma_\mu u) s \}$	1	+1
		Σ^{*0}	$\frac{1}{\sqrt{3}} \epsilon \{ (u^T C \gamma_\mu d) s + (d^T C \gamma_\mu s) u + (s^T C \gamma_\mu u) d \}$	1	0
		Σ^{*-}	$\frac{1}{\sqrt{3}} \epsilon \{ 2(d^T C \gamma_\mu s) d + d^T C \gamma_\mu d) s \}$	1	-1
$s = 2$		Ξ^{*0}	$\frac{1}{\sqrt{3}} \epsilon \{ 2(s^T C \gamma_\mu u) s + (s^T C \gamma_\mu s) u \}$	1/2	+1/2
		Ξ^{*-}	$\frac{1}{\sqrt{3}} \epsilon \{ 2(s^T C \gamma_\mu d) s + (s^T C \gamma_\mu s) d \}$	1/2	-1/2
$s = 3$		Ω^-	$\epsilon(s^T C \gamma_\mu s) s$	0	0
$c = 1$	$s = 0$	Σ_c^{*++}	$\frac{1}{\sqrt{3}} \epsilon \{ 2(u^T C \gamma_\mu c) u + u^T C \gamma_\mu u) c \}$	1	+1
		Σ_c^{*+}	$\frac{1}{\sqrt{3}} \epsilon \{ (u^T C \gamma_\mu d) c + (d^T C \gamma_\mu c) u + (c^T C \gamma_\mu u) d \}$	1	0
		Σ_c^{*0}	$\frac{1}{\sqrt{3}} \epsilon \{ 2(d^T C \gamma_\mu c) d + d^T C \gamma_\mu d) c \}$	1	-1
$s = 1$		Ξ_c^{*+}	$\frac{1}{\sqrt{3}} \epsilon \{ (u^T C \gamma_\mu s) c + (s^T C \gamma_\mu c) u + (c^T C \gamma_\mu u) s \}$	1/2	+1/2
		Ξ_c^{*0}	$\frac{1}{\sqrt{3}} \epsilon \{ (d^T C \gamma_\mu s) c + (s^T C \gamma_\mu c) d + (c^T C \gamma_\mu d) s \}$	1/2	-1/2
$s = 2$		Ω_c^{*0}	$\frac{1}{\sqrt{3}} \epsilon \{ 2(s^T C \gamma_\mu c) s + (s^T C \gamma_\mu s) c \}$	0	0
$c = 2$	$s = 0$	Ξ_{cc}^{*++}	$\frac{1}{\sqrt{3}} \epsilon \{ 2(c^T C \gamma_\mu u) c + (c^T C \gamma_\mu c) u \}$	1/2	+1/2
		Ξ_{cc}^{*+}	$\frac{1}{\sqrt{3}} \epsilon \{ 2(c^T C \gamma_\mu d) c + (c^T C \gamma_\mu c) d \}$	1/2	-1/2
		Ω_{cc}^{*+}	$\frac{1}{\sqrt{3}} \epsilon \{ 2(c^T C \gamma_\mu s) c + (c^T C \gamma_\mu c) s \}$	0	0
$c = 3$	$s = 0$	Ω_{ccc}^{++}	$\epsilon(c^T C \gamma_\mu c) c$	0	0

Table 3: Interpolating fields of $SU(4)$ 20-plet (“decuplet-type”) baryons with spin 3/2. Throughout the color indices are suppressed, i.e. $\epsilon(x^T C \gamma_\mu y) z$ is to be read as $\epsilon_{abc} (x_a^T C \gamma_\mu y_b) z_c$.

charm	strange	baryon	interpolating field	I	I_z
$c = 0$	$s = 1$	Λ^0	$\frac{1}{\sqrt{3}} \epsilon \{ (u^T C \gamma_5 d) s + (s^T C \gamma_5 u) d + (d^T C \gamma_5 s) u \}$	0	0
$c = 1$	$s = 0$	Λ_c^+	$\frac{1}{\sqrt{3}} \epsilon \{ (u^T C \gamma_5 d) c + (c^T C \gamma_5 u) d + (d^T C \gamma_5 c) u \}$	0	0
		$\Xi_c''^+$	$\frac{1}{\sqrt{3}} \epsilon \{ (u^T C \gamma_5 s) c + (c^T C \gamma_5 u) s + (s^T C \gamma_5 c) u \}$	1/2	+1/2
		$\Xi_c''^0$	$\frac{1}{\sqrt{3}} \epsilon \{ (d^T C \gamma_5 s) c + (c^T C \gamma_5 d) s + (s^T C \gamma_5 c) d \}$	1/2	-1/2

Table 4: Interpolating fields of $SU(4)$ $\bar{4}$ -plet (“new-type”) baryons. Throughout the color indices are suppressed, i.e. $\epsilon(x^T C \gamma_5 y) z$ is to be read as $\epsilon_{abc} (x_a^T C \gamma_5 y_b) z_c$.

the $c = 2$ second floor which transforms as a 3 [lines 17-19], and the $c = 3$ one-point summit of the pyramid [line 20]. Here we adopt the rule that in the 20-plet the diquark $(x^T C \gamma_\mu y)$ is symmetric under the interchange $x \leftrightarrow y$.

The $\bar{4}$ -plet decomposes into a $c = 0$ ground floor which is an $SU(3)$ singlet [line 1 in Tab. 4], and a $c = 1$ first floor which transforms as a $\bar{3}$ [lines 2-4]. In the former case the construction is based on the requirement that $\Sigma^0 \propto (us)d + (ds)u$, $\Lambda^0 \equiv \Lambda_8^0 \propto 2(ud)s + (us)d - (ds)u$, and $\Lambda'^0 \equiv \Lambda_0^0 \propto (ud)s + (su)d + (ds)u$ would be mutually orthogonal. In the latter case the interpolator is antisymmetric under the interchange of the two non-charmed quarks, if we adopt the rule that the diquark $(x^T C \gamma_5 y)$ is antisymmetric under the interchange $x \leftrightarrow y$.

References

- [1] Z. Fodor and C. Hoelbling, Rev. Mod. Phys. **84**, 449 (2012) [arXiv:1203.4789].
- [2] B. Sheikholeslami and R. Wohlert, Nucl. Phys. B **259**, 572 (1985).
- [3] M. Luscher, S. Sint, R. Sommer and P. Weisz, Nucl. Phys. B **478**, 365 (1996) [hep-lat/9605038].
- [4] T.A. DeGrand, A. Hasenfratz and T.G. Kovacs [MILC Collaboration], hep-lat/9807002.
- [5] C.W. Bernard and T. DeGrand, Nucl. Phys. Proc. Suppl. **83**, 845 (2000) [hep-lat/9909083].
- [6] M. Stephenson, C. DeTar, T.A. DeGrand and A. Hasenfratz, Phys. Rev. D **63**, 034501 (2001) [hep-lat/9910023].
- [7] J.M. Zanotti *et al.* [CSSM Collab.], Phys. Rev. D **65**, 074507 (2002) [hep-lat/0110216].
- [8] T. DeGrand, A. Hasenfratz and T.G. Kovacs, Phys. Rev. D **67**, 054501 (2003) [hep-lat/0211006].
- [9] S. Capitani, S. Durr and C. Hoelbling, JHEP **0611**, 028 (2006) [hep-lat/0607006].
- [10] S. Durr, Comput. Phys. Commun. **180**, 1338 (2009) [arXiv:0709.4110].
- [11] S. Durr, Z. Fodor, C. Hoelbling, S. D. Katz, S. Krieg, T. Kurth, L. Lellouch and T. Lippert *et al.*, JHEP **1108**, 148 (2011) [arXiv:1011.2711].
- [12] S. Durr and G. Koutsou, Phys. Rev. D **83**, 114512 (2011) [arXiv:1012.3615].
- [13] W. Bietenholz and I. Hip, Nucl. Phys. B **570**, 423 (2000) [hep-lat/9902019].
- [14] W. Bietenholz, M. Gockeler, R. Horsley, Y. Nakamura, D. Pleiter, P. E. L. Rakow, G. Schierholz and J. M. Zanotti, Phys. Lett. B **687**, 410 (2010) [arXiv:1002.1696].
- [15] G. S. Bali *et al.* [QCDSF Collab.], Phys. Rev. Lett. **108**, 222001 (2012) [arXiv: 1112.3354].
- [16] S. Gusken, U. Low, K. H. Mutter, R. Sommer, A. Patel and K. Schilling, Phys. Lett. B **227**, 266 (1989).
- [17] G. Colangelo *et al.* [FLAG], Eur. Phys. J. C **71**, 1695 (2011) [arXiv:1011.4408].
- [18] K. Nakamura *et al.* [Particle Data Group Collab.], J. Phys. G G **37**, 075021 (2010).
- [19] L. Del Debbio, L. Giusti, M. Luscher, R. Petronzio and N. Tantalo, JHEP **0602**, 011 (2006) [hep-lat/0512021].
- [20] F. X. Lee and D. B. Leinweber, Nucl. Phys. Proc. Suppl. **73**, 258 (1999) [hep-lat/9809095].
- [21] D. B. Leinweber, W. Melnitchouk, D. G. Richards, A. G. Williams and J. M. Zanotti, Lect. Notes Phys. **663**, 71 (2005) [nucl-th/0406032].
- [22] K. C. Bowler *et al.* [UKQCD Collab.], Phys. Rev. D **54**, 3619 (1996) [hep-lat/9601022].
- [23] R. G. Edwards, J. J. Dudek, D. G. Richards and S. J. Wallace, Phys. Rev. D **84**, 074508 (2011) [arXiv:1104.5152].
- [24] R. Lewis, N. Mathur and R. M. Woloshyn, Phys. Rev. D **64**, 094509 (2001) [hep-ph/0107037].
- [25] N. Mathur, R. Lewis and R. M. Woloshyn, Phys. Rev. D **66**, 014502 (2002) [hep-ph/0203253].
- [26] J. M. Flynn *et al.* [UKQCD Collab.], JHEP **0307**, 066 (2003) [hep-lat/0307025].
- [27] H. Na and S. Gottlieb, PoS LATTICE **2008**, 119 (2008) [arXiv:0812.1235].

- [28] L. Liu, H. -W. Lin, K. Orginos and A. Walker-Loud, Phys. Rev. D **81**, 094505 (2010) [arXiv:0909.3294].
- [29] H. -W. Lin, S. D. Cohen, L. Liu, N. Mathur, K. Orginos and A. Walker-Loud, Comput. Phys. Commun. **182**, 24 (2011) [arXiv:1002.4710].
- [30] D. Mohler and R. M. Woloshyn, Phys. Rev. D **84**, 054505 (2011) [arXiv:1103.5506].
- [31] Y. Namekawa *et al.* [PACS-CS Collab.], Phys. Rev. D **84**, 074505 (2011) [arXiv:1104.4600].
- [32] H. -W. Lin, Chin. J. Phys. **49**, 827 (2011) [arXiv:1106.1608].
- [33] C. Alexandrou, J. Carbonell, D. Christaras, V. Drach, M. Gravina and M. Papinutto, arXiv:1205.6856 [hep-lat].
- [34] R. A. Briceno, H. -W. Lin and D. R. Bolton, arXiv:1207.3536 [hep-lat].
- [35] P. Hasenfratz and F. Niedermayer, Nucl. Phys. B **414**, 785 (1994) [hep-lat/9308004].
- [36] W. Bietenholz and U. J. Wiese, Nucl. Phys. B **464**, 319 (1996) [hep-lat/9510026].
- [37] P. Hasenfratz, S. Hauswirth, K. Holland, T. Jorg, F. Niedermayer and U. Wenger, Int. J. Mod. Phys. C **12**, 691 (2001) [hep-lat/0003013].
- [38] P. Hasenfratz, S. Hauswirth, T. Jorg, F. Niedermayer and K. Holland, Nucl. Phys. B **643**, 280 (2002) [hep-lat/0205010].
- [39] M. F. L. Golterman and J. Smit, Nucl. Phys. B **245**, 61 (1984).
- [40] D. H. Adams, Phys. Lett. B **699**, 394 (2011) [arXiv:1008.2833].
- [41] C. Hoelbling, Phys. Lett. B **696**, 422 (2011) [arXiv:1009.5362].
- [42] M. Creutz, T. Kimura and T. Misumi, JHEP **1012**, 041 (2010) [arXiv:1011.0761].
- [43] P. de Forcrand, A. Kurkela and M. Panero, JHEP **1204**, 142 (2012) [arXiv:1202.1867].
- [44] S. Durr and G. Koutsou, Phys. Rev. Lett. **108**, 122003 (2012) [arXiv:1108.1650].